CFD CODE – A USEFUL TOOL
FOR THE TURBOMACHINERY DESIGNER

RYSZARD CHODKIEWICZ, KRZYSZTOF SOBCZAK,
ADAM PAPIERSKI AND TOMASZ BORZĘCKI

Technical University of Lodz, Institute of Turbomachinery,
Wolczanska 219/223, 93-005 Lodz, Poland
rchod@ck-sg.p.lodz.pl

Abstract: The presentation of CFX-TASCflow code possibilities for the turbomachinery design is the main aim of this study. In the first part of the work the compressor redesign process is presented. Next, CFX-TASCflow possibilities in predicting unstable operating conditions (surge) are shown. The one-stage, radial blower installed in the Institute of Turbomachinery TU of Lodz has been chosen owing to the available numerous experimental data. The pump calculations discussed in the third part concern a comparison of different turbulence models with the experimental results. In the last part devoted to the turbine redesign, the code usefulness is proved on the examples of the last stage design process.

Keywords: CFD, radial compressor, radial pump, axial flow turbine

1. Introduction

The turbomachinery design process is based on one-dimensional (1D) determination of the meridional channel and blade shape. Before 3D methods of the fluid flow simulation were applied, the verification of the construction quality was possible only on the test stand in the case of mass-production or during the operation for piece production. Experimental investigations of a prototype gave information about the machine operation and were the basis of the modifications, which improved the product quality. However, prototype investigations are very expensive, especially in the case of turbomachinery. The utilization of three-dimensional (3D) methods of fluid flow simulations allows one to reduce the range of experimental investigations or even to eliminate them.

3D methods (*e.g.* CFX-TASCflow) allow one to determine the flow and thermodynamic parameter fields, which is often not possible by the experimental way. The analysis of these fields is the basis to determine the necessary improvements leading to optimization of the turbomachinery channel shape. Due to relatively low

(in comparison with experimental investigations) costs of numerical simulations, it is possible to execute improvement – verification cycles many times and, as a result, to obtain an optimal construction.

2. Radial compressor redesign

An example of the 3D method utilization in the turbomachinery optimization process is a rotor of the radial compressor. The machine was modernized in such a way that the body was not changed. The basic shape of a new rotor was determined by 1D methods. The CFX-TASCFLOW code was used to calculate the fluid flow through the rotor flow passage [1]. Numerical investigations of the flow revealed wide zones of vortices at the suction side of the blade and at the outlet of the rotor. A correction of the channel meridional shape was performed. Because of the original machine body limitations, it was not possible to eliminate the vortices zones but they were significantly reduced. The relative total pressure distributions: in the middle of the rotor passage (in the meridional cross-section) and in the half of the blade height (B2B), before and after modification (Figure 1 and Figure 2) present the zones of the vortices in the passage.

Advantages of 3D methods of the fluid flow simulation were revealed also in the case of the inlet angle correction. The angles of the leading edge obtained from 1D methods were proper only in the middle of the blade height. Significant differences were revealed between the velocity vector direction and blade angle at the hub and the shroud. At the hub, at the suction side of the blade and close to the leading edge, a small vortex was observed, similarly as at the shroud at the pressure side (Figure 3). After the correction of the leading edge angles, the inflow of the fluid on the blade is proper.

3. Phenomena responsible for the unsteady radial compressor operation

3.1. 1I1.76 compressor geometry

The investigated compressor is a one-stage radial blower mounted in the compact arrangement (Figure 4). The nominal pressure ratio is equal to $\pi = 1.52$ for the nominal mass flow equal to $\dot{m} = 16\,\mathrm{kg/s}$ (under normal inlet conditions). The rotor wheel is radial with the blade number equal to 21. The blade outlet angle β_2^* is equal to $90°$. The blade inlet angle β_1^* varies along the radius. The rotor rotational speed is equal to 5775 rpm. An adjustable inlet guide vane is located downstream of the rotor. The investigation range was limited to the case of the inlet guide vane with the axial position and a vaneless diffuser [2–5].

3.2. Geometry

For the geometrical data input, AUTOCAD was used. Proper AUTOLISP procedures outputted data in the form suitable for the TURBOGRID program used for the grid generation. TURBOGRID allows one to control the grid quality by the data exchange with the Graphical User Interface of the CFX-TASCFLOW code.
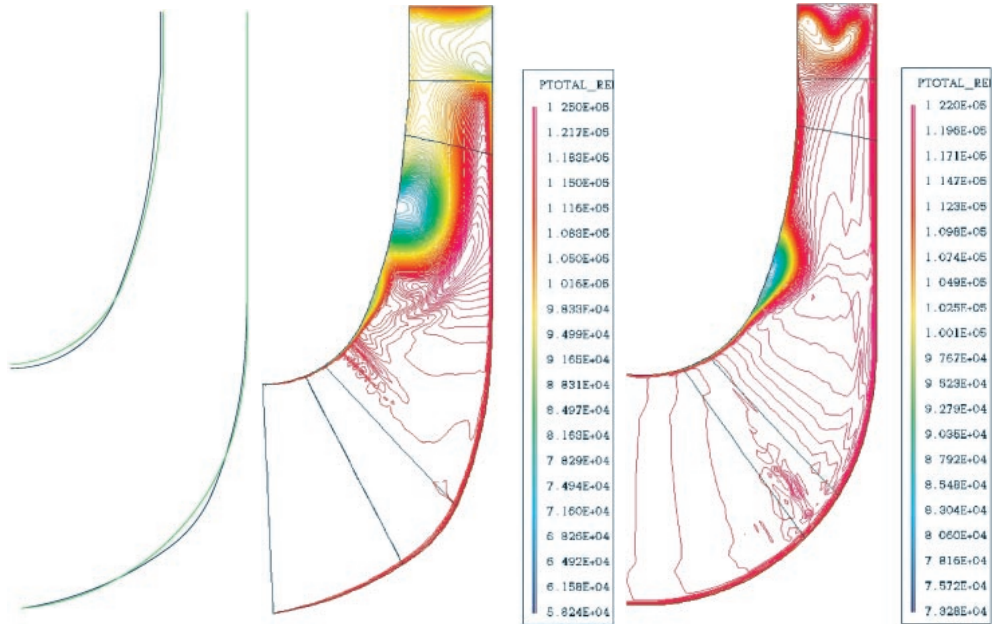
Figure 1. Meridional cross-section of the channel: left – channel shape before (black line) and after modification (green line); middle and right – relative total pressure distribution before and after modification
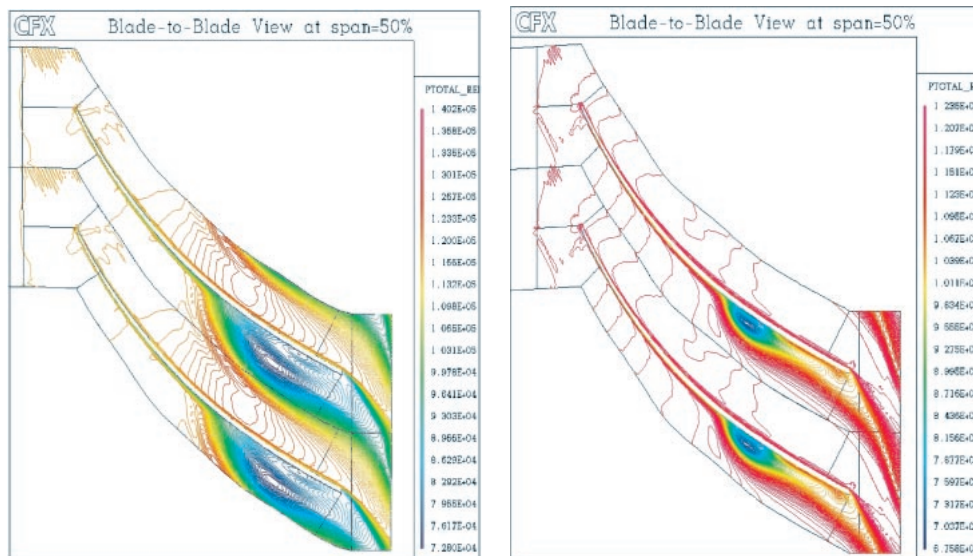

Figure 2. Blade-to-blade (B2B) cross-section of the channel in the middle of the blade height: left – before modification; right – after modification
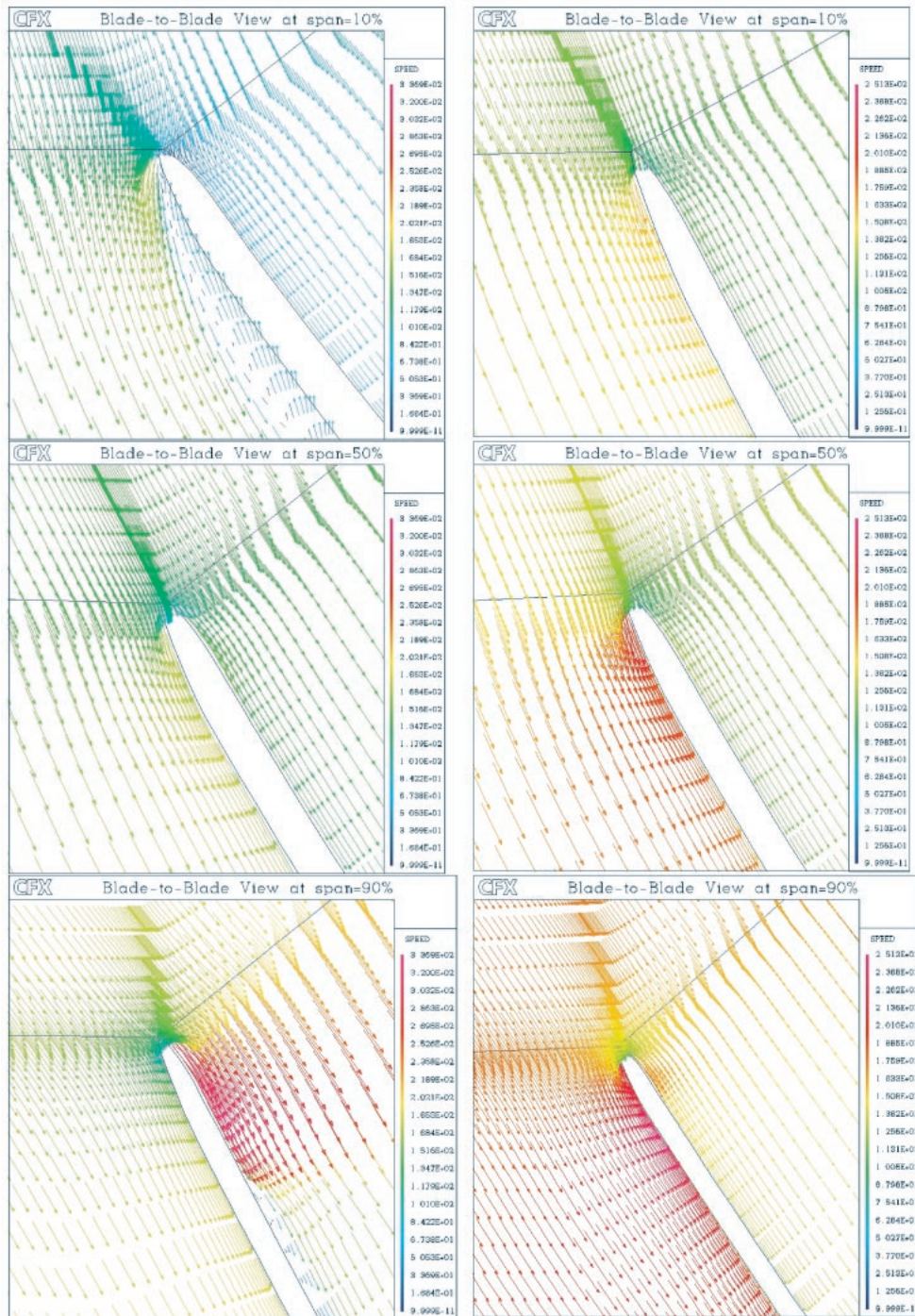
Figure 3. Velocity vector distributions at the inlet of the rotor before (left column) and after the correction (right column) in the blade-to-blade (B2B) cross-section for 10, 50 and 90% of the blade height
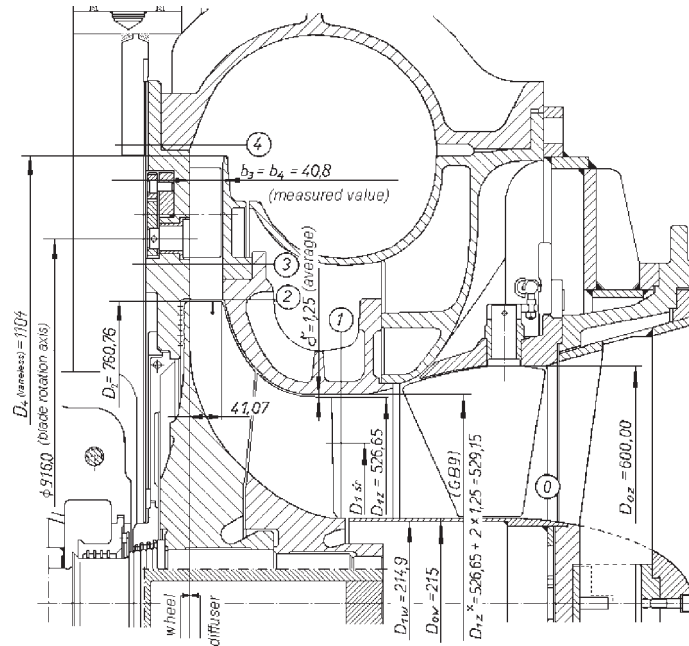
Figure 4. Meridional section of the 1I1.76 Compressor

3.3. Boundary conditions

It is recommended to use one of the boundary conditions in Table 1 for the task description in CFX-TASCFLOW.

Table 1. Different boundary conditions which can be used in CFX-TASCFLOW

No.	Inlet	Outlet
1	Mass flow $\dot{m}$, velocity $\vec{v}$	Static pressure p
2	Total pressure p_e	Mass flow $\dot{m}$
3	Total pressure p_e	Static pressure p

Boundary conditions No. 2 from Table 1 were used in the calculations:

1. total pressure at the inlet $p_{e\alpha} = 0.99$ bar;
2. outlet mass flow of the air was changed in the range of 8–24 kg/s.

Apart from the boundary conditions at the outlet and inlet, the following conditions are assumed:

- boundary conditions on the walls;
- periodicity conditions on the surfaces located in the centers of two adjacent channels;
- connection conditions for two close surfaces (the first one in the stationary frame and the second one in the rotating frame).

On the walls not only the lack of the mass and momentum transfer is assumed, but the wall is treated as adiabatic. The periodicity conditions can be posed on the adjacent walls (the same surface – a possible parallel or angular transformation).
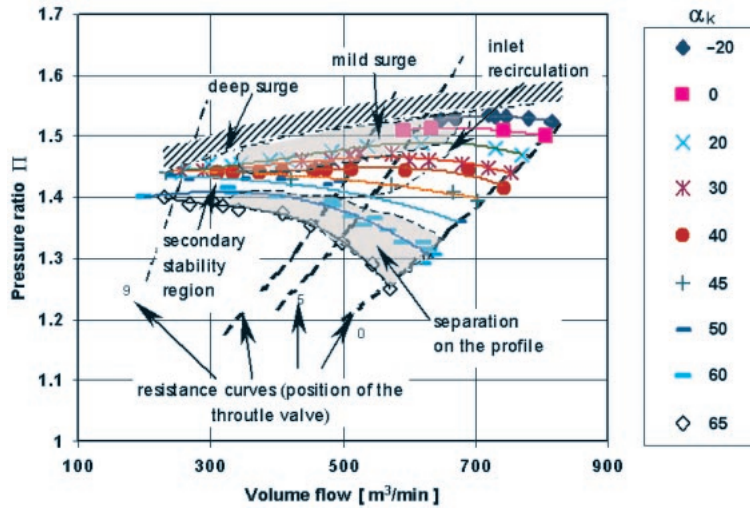
Figure 5. Compressor characteristics obtained experimentally (pressure ratio and compressor power versus inlet mass flow, α_k – stator blade-angle setting)

The calculations are made like for the steady flow – it means the instantaneous stator and rotor position is taken in the calculations (frozen rotor interface) and the stationary frame of reference is recalculated onto the rotational frame of reference on the connection surface.

3.4. Range and results of the calculations

The CFX-TASCflow code is a useful tool not only for the turbomachinery design under nominal operating conditions, but can be also used to predict turbomachinery characteristics. The calculation has been made for the mass flow range enclosed by the measured characteristics presented in Figure 5.

The mass flow calculated by CFX-TASCflow is significantly lower than the mass flow for which the measurements were possible. It shows that CFX-TASCflow allows one to calculate a flow for unstable conditions, *i.e.* in the region where surge appears as well.

3.5. Phenomena responsible for surge

Simulations for low mass flows allow one to reveal details of phenomena, which cause the compressor unstable operation. The inlet recirculation, separation zone and other phenomena responsible for surge were discovered during the investigations and their evolution with the mass flow changes was observed.

3.5.1. Inlet recirculation

The inlet recirculation is a stationary phenomenon. It appears at the radial machine inlet with a pressure growth at the outlet, *e.g.* caused by closing the throttle valve or by a growth of the grid resistance. That phenomenon is usually the first symptom of the unstable compressor operation [6]. The evolution of the inlet recirculation zone with the mass flow changes is presented in Figure 6.

This recirculation lasts very long – up to the mass flow equal to 12 kg/s. The phenomenon disappears when the mass flow exceeds 14 kg/s. However, the inlet
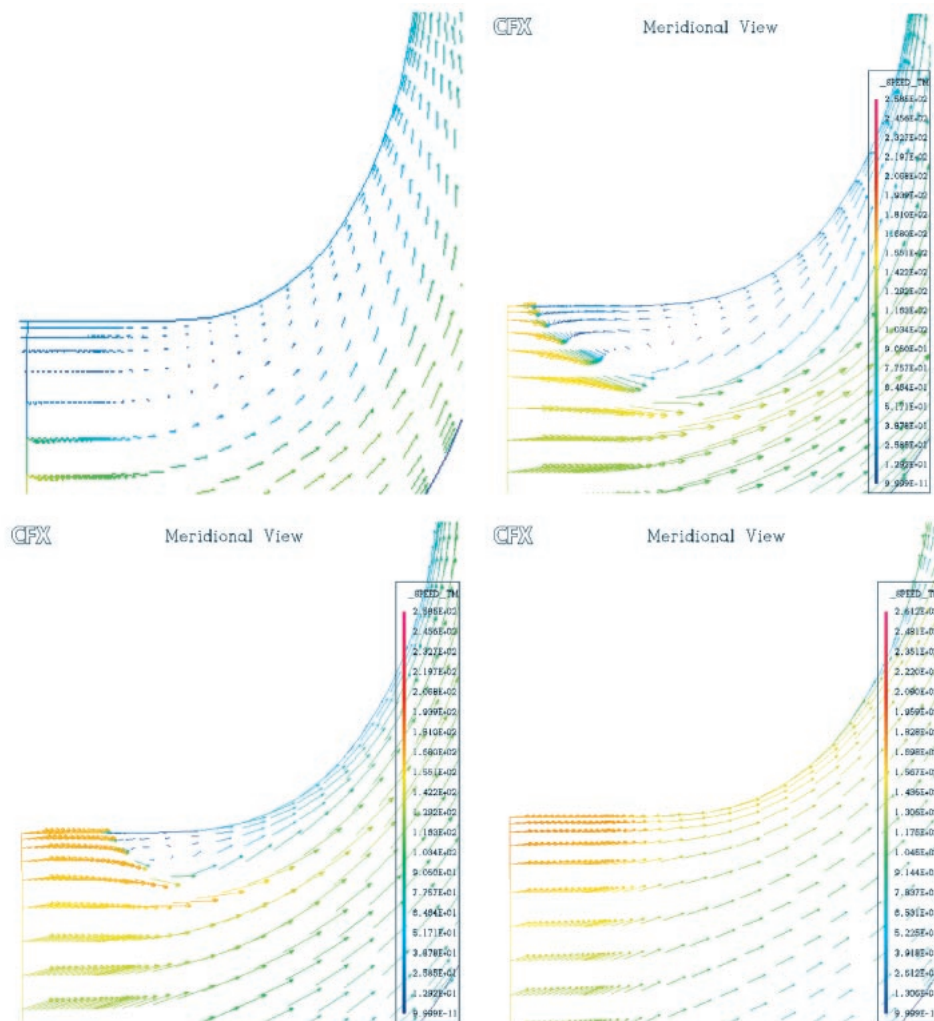
Figure 6. Evolution of the inlet recirculation zone with the mass flow changes

recirculation unprofitably influences the compressor working conditions and it is not equivalent to the surge appearance, although in a compressor with a high-pressure ratio, it can lead to intensive surge.

3.5.2. Separation in the vaneless diffuser

Separation in the vaneless diffuser is another phenomenon disclosed in the calculations. That kind of reverse flows depends strongly on the inlet swirl. It is usually assumed that this phenomenon appears when $\operatorname{tg}\alpha < 0.25$ [7]. In the calculations, this separation was discovered for the lowest mass flow only. The fact that this phenomenon does not exist for higher mass flows means that the diffuser was properly designed and it means that significantly high-pressure gradients do not appear in the channel.

In Figure 7 fewer details can be seen than in Figure 6, although it is visible that there are no other regions in which the velocity vector directions differ from the main flow direction.
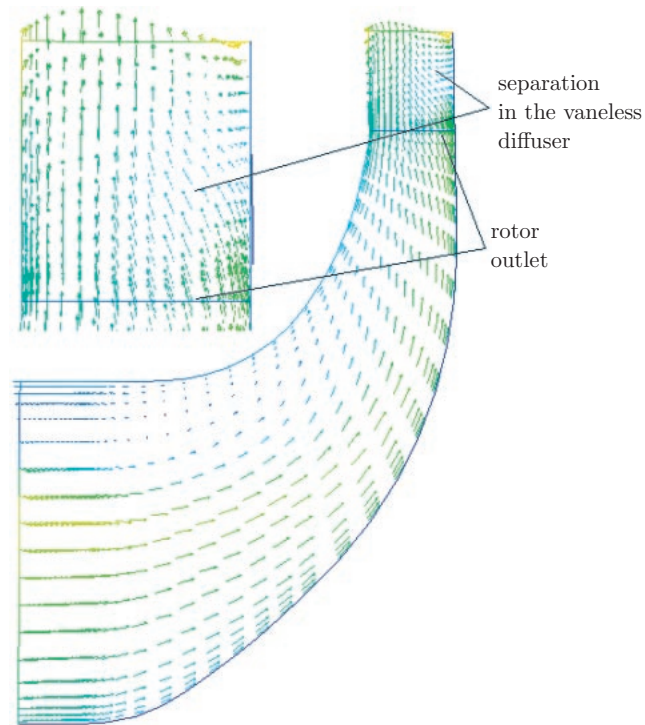
separation
in the vaneless
diffuser

rotor
outlet

Figure 7. Separation in the vaneless diffuser, $m = 8$ kg/s, rotating frame,
center of the B2B channel

3.5.3. Total pressure distributions and losses

The observation of total pressure distributions informs one about the flow disturbances and losses. The regions with lower total pressure values are equivalent to the regions in which the generated losses are significantly higher than in the remaining part of the flow channel.

The total pressure loss distribution in the meridional compressor section and in the rotating frame is presented in Figure 8. The influence of the inlet recirculation is clearly visible here, and it occupies a significant part of the flow channel. The region with lower total pressure values appears in the place where the separation in the vaneless diffuser exists.

Higher total pressure values confirming the lack of disturbances appear only in the region close to the compressor rear wall.

In Figure 9 the total pressure distributions at the S1 surfaces (blade-to-blade) located at the outer region (a), at the mean blade height (b), and at the inner region (c) are presented. In the outer region, higher total pressure values are observed at the suction side of the blade close to the outlet. In the central region, that domain is significantly wider and in the region close to the rear wall it occupies almost the whole channel. The influence of the inlet recirculation and separation in the vaneless diffuser are especially visible here, which is confirmed by lower total pressure values at the compressor inlet.
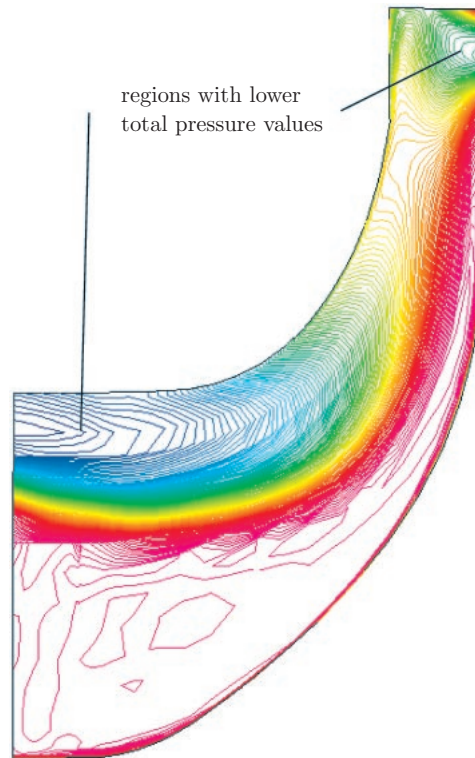
Figure 8. Total pressure loss distribution in the meridional section of the rotor in the rotating frame $m = 8\,\mathrm{kg/s}$ (center of the B2B channel)

3.6. Calculations in the compressor operating point

The majority of the disadvantageous phenomena, which exists at lower mass flows, disappear in the compressor operating point. First of all, the separation in the vaneless diffuser disappears for mass flows higher than $12\,\mathrm{kg/s}$.

The inlet recirculation is not observed at the compressor operating point. Vectors at the meridional section are parallel to the main flow direction. However, not all phenomena responsible for the loss generation disappear.

3.6.1. Velocity vectors in the flow

The velocity vectors in the meridional view for the nominal air mass flow are presented in Figure 10. A significant flow acceleration is visible at the rotor inlet in the region close to the blade tip. Lower velocity values dominate in the region close to the hub. The stream accelerates distinctly at the rotor outlet and the velocities in that region are close to the velocity directions and values in the main flow. However, a region with lower velocities can be seen at the blade tip. The width of that region increases along the flow direction.

3.6.2. Separation in the rotor blade-to-blade channel

The velocity distributions in the region close to the blade tip $(x/L = 0.95)$ for four different mass flows are presented in Figure 11. It is clearly visible that the flow, uniform for the compressor operating point ($16\,\mathrm{kg/s}$), is deformed with an air mass flow decrease. A vortex that is not so large at the beginning transforms into the flow

higher total pressure
value region appears
at the rotor outlet,
in the domain close to
the pressure side
of the blade

region with lower
total pressure values
extends widely
in the domain close to
the blade suction side

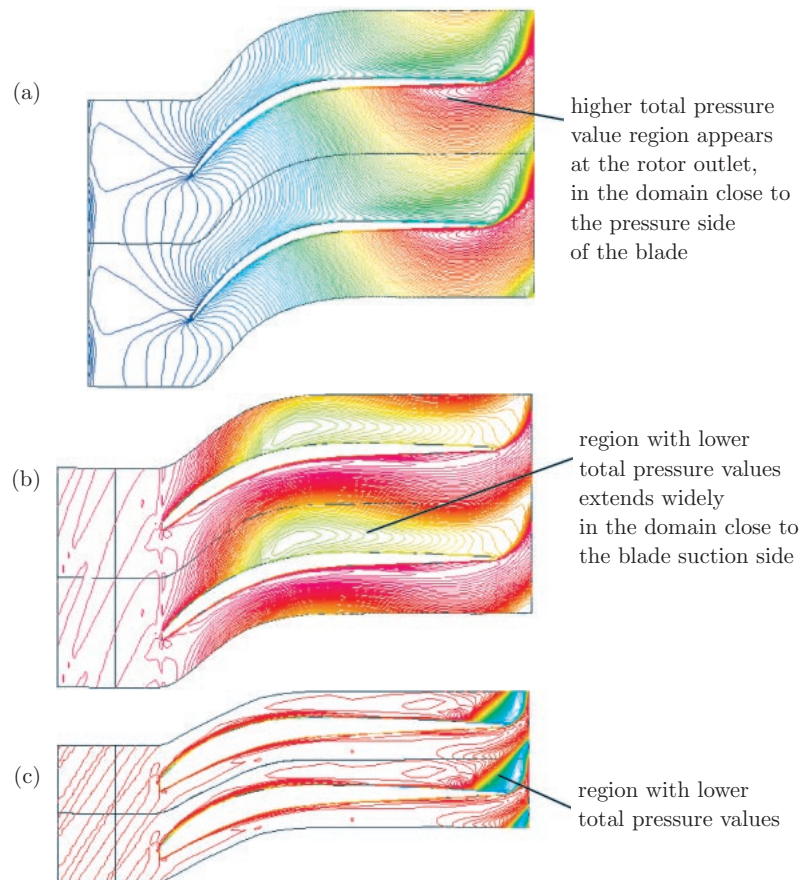region with lower
total pressure values

Figure 9. Total pressure distributions on the developed view of the stream surfaces,
close to the tip, hub and in the central part of the blade: (a) at the blade tip,
(b) at the mean blade height, (c) at the rear wall

with the direction opposite to the main flow direction (classical inlet recirculation). In the regions closer to the hub, the air flows in the right direction and is consistent with the direction forced by the blade shape.

As results from Figure 12, an additional vortex appears at the suction side of the blade in the region close to the blade tip. That vortex is the source of additional losses. The places in which these losses are generated are especially visible in the figures presenting total pressure distributions. The differences between values and distributions of total pressure losses can be clearly seen if one compares Figure 9 (part 1) with Figure 13 (different air mass flows). In the region close to the rear wall and at the half of the blade height, significantly higher losses occur at the blade wake. At the blade center on the pressure side, a secondary flow starts to occur. An influence of that secondary flow is strongly disclosed at the blade tip (Figure 13).

The secondary flow is best observed at the section perpendicular to the main flow. The vortex coming from secondary flows, appearing at the blade suction side, is clearly seen in Figure 14. At the pressure side, vortices cannot be seen – only a distinctly oriented flow from the pressure side to the channel center occurs.
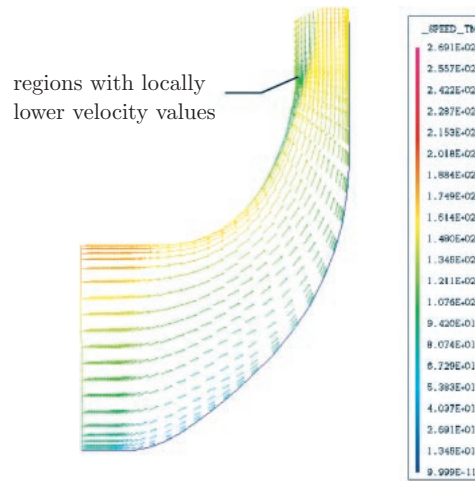
Figure 10. Velocity vectors in the meridional view of the compressor
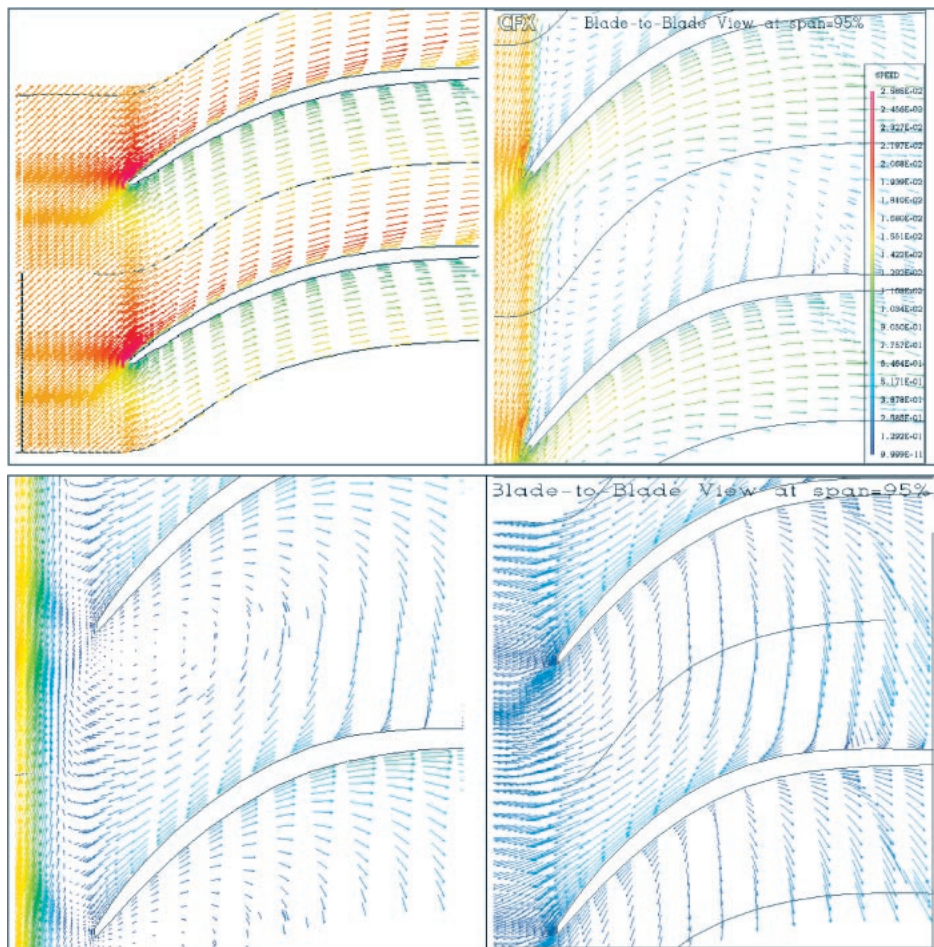for the nominal air mass flow

Figure 11. Velocity vector view in the region close to the blade tip

Figure 12. Velocity vectors view on the S1 surface (blade profile mark in the center of the drawing) close to the blade tip. At the suction side, secondary flow vortex clearly visible ($m = 16$ kg/s)
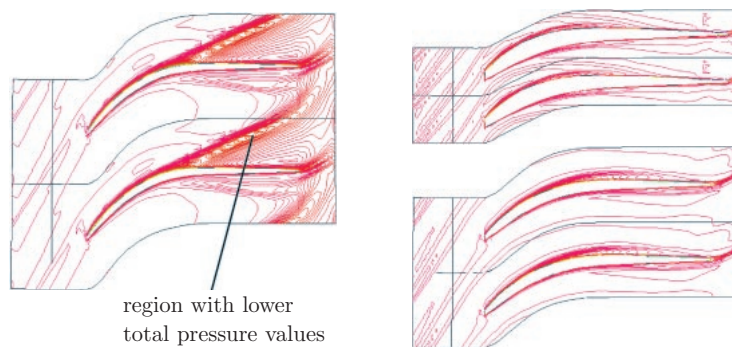

region with lower
total pressure values

Figure 13. Total pressure distributions on the S1 surface (blade-to-blade), $m = 16$ kg/s
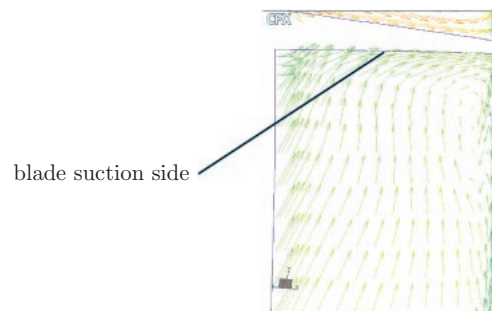

blade suction side

Figure 14. Secondary flow disclosed at the suction side of the blade

3.7. Comparison between the computations and experiments

The assessment and comparison of the computations with the experiment was difficult, especially because the experimental range in the region of unstable operation was not as wide as the calculations. On the experimental stand:

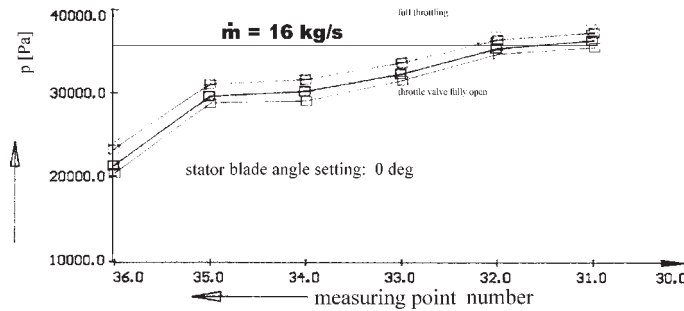- it was impossible to get the air mass flow lower than 12.5 kg/s due to the compressor surge;

Figure 15. Static pressure distribution (measurement) along the diffuser rear wall
for the stator blade angle setting = 0° (point numbers as a radius function:
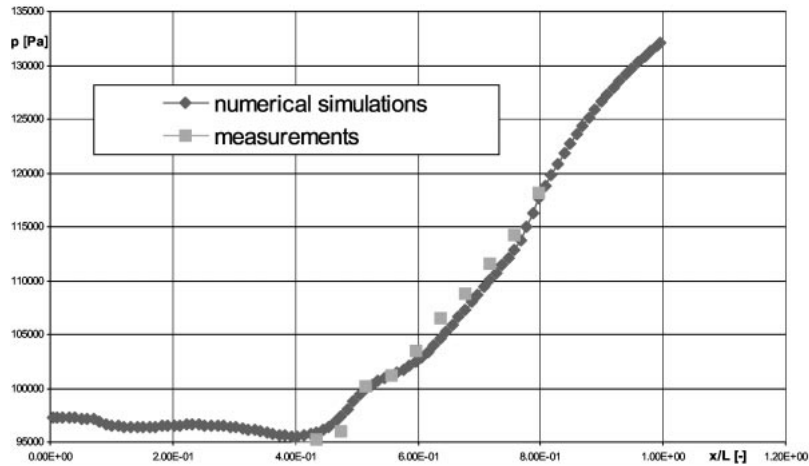point No. 31 – diffuser outlet, point No. 36 – rotor outlet)

Figure 16. Static pressure distribution at the compressor blade tip

- it was impossible to get the air mass flow higher than 17 kg/s due to the resistances of the air grid cooperating with the compressor.

The calculation domain was additionally limited to the inlet stator, rotor and vaneless diffuser due to the PC class computer limitations. The original compressor stand was supplied additionally with a volute and a conical outlet diffuser joined with that volute.

The static pressure distributions on the diffuser rear wall were measured as well. These distributions compared with the calculated diffuser outlet pressure prove the quality of the computations (Figure 15).

The measurements presented in Figure 16 show that the diffuser outlet pressure for the air mass flow equal to 16 kg/s is equal to 1.357 bar. That value can be checked by the comparison with the calculation results presented in Table 2. The computed static pressure at the vaneless diffuser outlet is equal to 1.322 bar. It means that the relative pressure description error in the compressor operating point is equal to:

$$\delta p = \frac{1.357 - 1.322}{1.357} \cdot 100\% \approx 2.6\%$$

Table 2. Calculated compressor characteristics

$\dot{m}$	$\pi_{\text{diffuser inlet}}$	$p_{\text{diffuser outlet}}$	c_{diffuser}	c_{outlet}	π_{total}	Notices
[kg/s]	[–]	[bar]	[m/s]	[m/s]	[–]	
8.0	1.3604	1.34680	138	69.2	1.4373	
8.8	1.3556	1.34211	142	71.2	1.4375	
9.6	1.3557	1.34211	142	71.2	1.4375	
12.0	1.3604	1.34685	149	74.9	1.4518	
14.0	1.3518	1.33827	161	81.1	1.4600	uncompressible flow
16.0	1.3355	1.32223	169	84.8	1.4546	
20.0	1.2996	1.28658	183	91.8	1.4408	
24.0	1.2509	1.23841	200	100.1	1.4200	
24.0	1.2878	1.27493	189	94.8	1.4388	compressible flow

It is really a good result and the comparison of the computations for uncompressible and compressible models shows that the latter one provides slightly higher-pressure values, which means that the relative pressure error should be lower.

The static pressure changes along the blade tip obtained both by the computations and by the measurements are presented in Figure 16. The measured data were available in the rotor only. A good accuracy can be seen here. The observed differences are contained in the measurement error range and can be caused by the measurement errors or by simplifications assumed in the calculations.

4. Incompressible, viscous 3D flow through the radial pump stage

The first stage of the radial pump was computed. The commercial CFX-TASCflow code was used in the flow simulations through the impeller, vaned diffuser channel, U-return channel and return vaned channel.
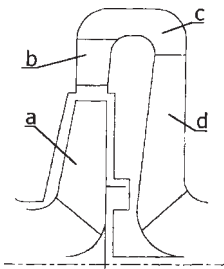

Figure 17. a – impeller, b – vaned diffuser channel, c – U-return channel, d – return vaned channel

The channel was projected by a structural grid with the total number of nodes equal to 180 000.

The following boundary conditions were posed in the calculations:

1. uniform velocity profile at the rotor inlet, without an inlet swirl (velocity profile integrated on the inlet surface yields the mass flow equal to the nominal mass flow per one channel;
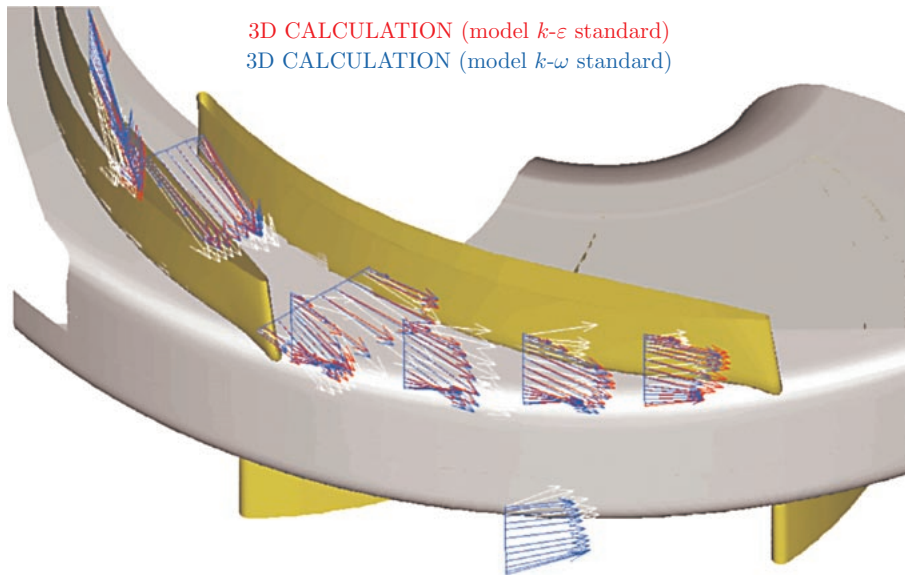
3D CALCULATION (model k-ε standard)
3D CALCULATION (model k-ω standard)

Figure 18. Velocity vector comparison in the probing places (perspective view)

3D CALCULATION (model k-ε standard)
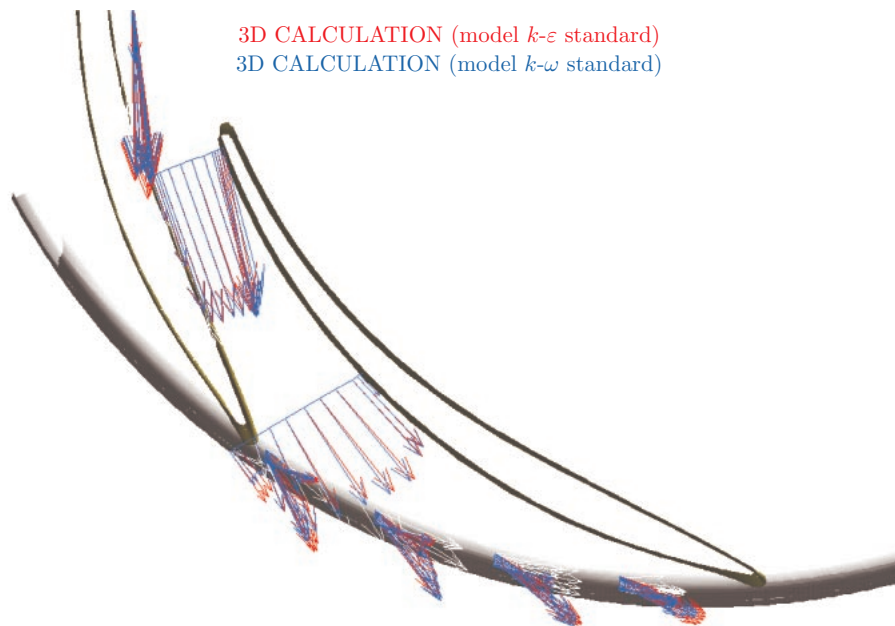3D CALCULATION (model k-ω standard)

Figure 19. Velocity vector comparison in the probing places (view along the axial direction)

2. turbulence intensity equal to 3% at the rotor inlet;
3. uniform, constant static pressure at the outlet surface of the return vaned channel;
4. velocity at the walls equal to zero.

At the transition border between the moving channel (rotor) and the remaining stationary part of the channel (both stators), the working medium parameters were
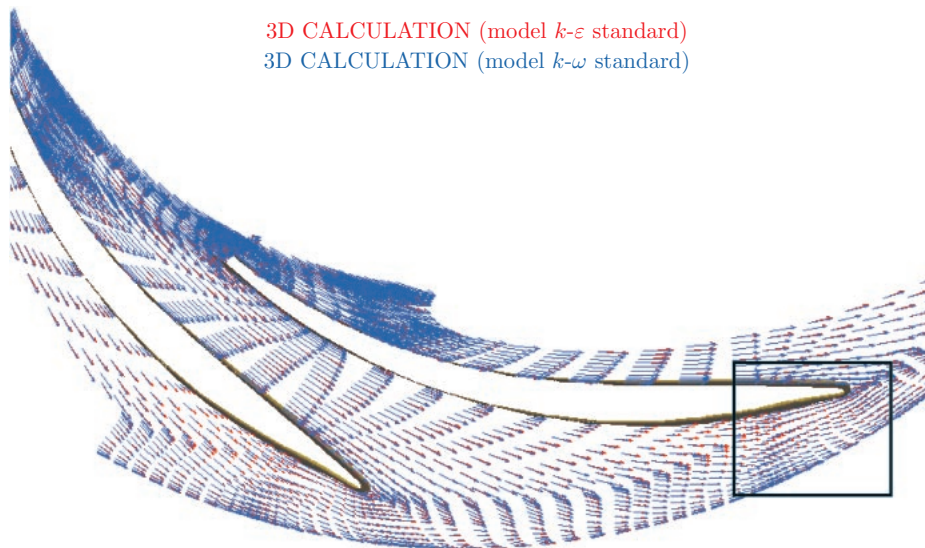
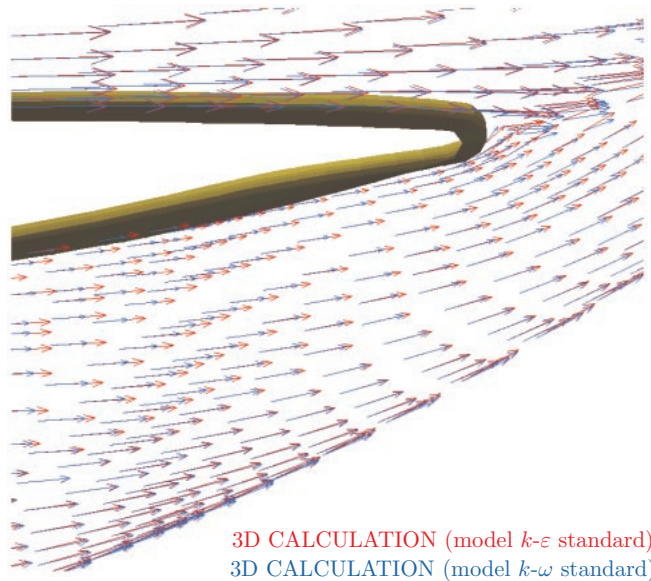**Figure 20.** Comparison of the velocity in the vaned diffuser channel

Figure 21. Zoomed area marked in Figure 20

averaged. The results of the calculations made for two turbulence models k-ε and k-ω were compared with the experimental data (investigations made in the Institute of Turbomachinery, TU of Lodz [8]). The velocity vectors in the places where the probes were located are presented in Figures 18 and 19 (green color refers to the experimental data). The calculations results were interpolated from the grid nodes into the points of measurement by using the method of reverse distances [9]. The agreement between the experiment and calculations was recognized as sufficient. The differences between both the turbulence models (k-ε: red, k-ω: blue) are shown in Figures 20 and 21. In the domains where the flow is undisturbed (no secondary flows and reverse flows),

3D CALCULATION (model k-ε standard)
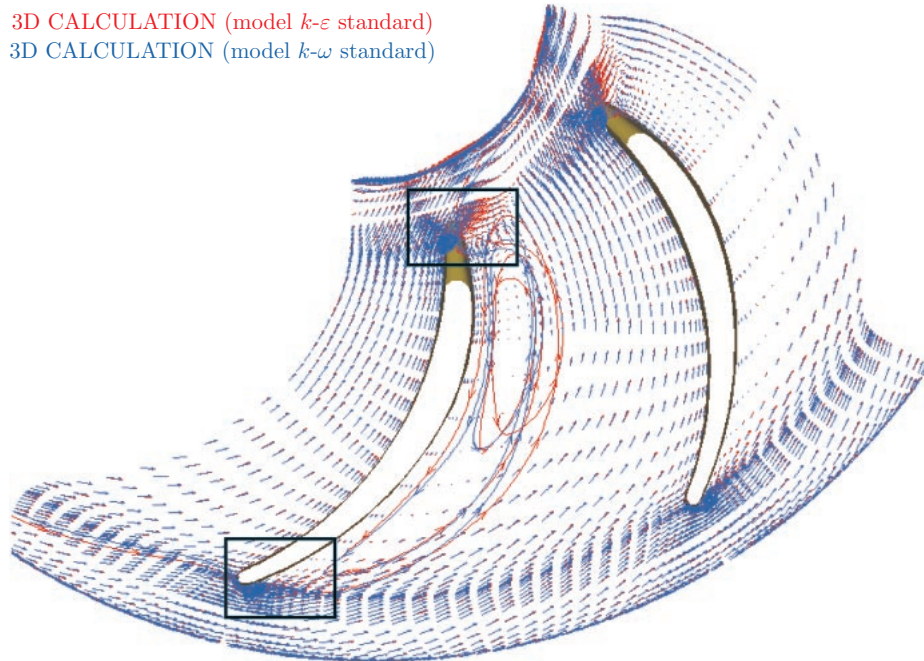3D CALCULATION (model k-ω standard)

Figure 22. Comparison of the velocity in the return vaned channel

3D CALCULATION (model k-ε standard)
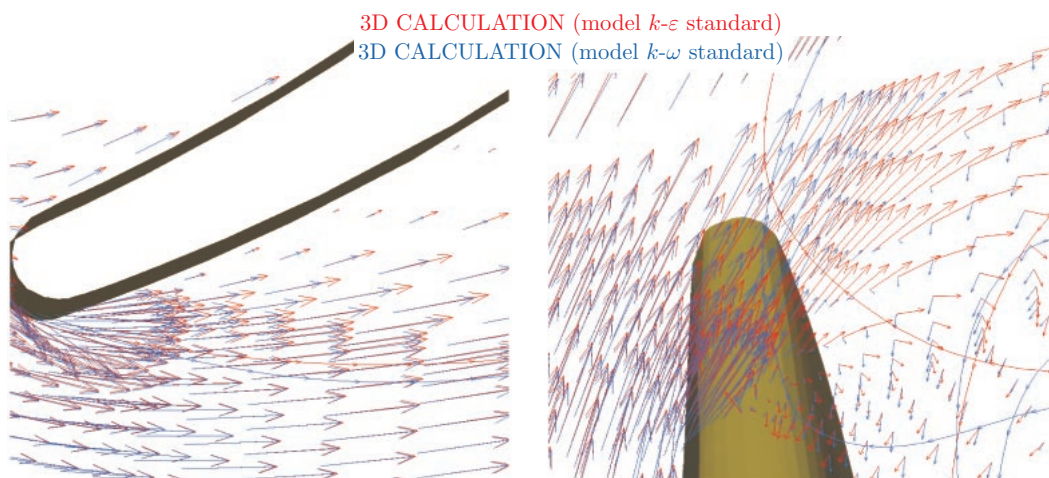3D CALCULATION (model k-ω standard)

Figure 23. Zoomed area marked
in Figure 22 (blade inflow)

Figure 24. Zoomed area marked
in Figure 22 (blade outflow)

these differences are almost insignificant. Significant differences are observed only in the places, where a well-developed boundary layer exists (Figure 21) In the k-ω model, the boundary layer thickness is from two to three times wider.

In the regions where the separations and reverse flows exist, the differences in the k-ω model exists and the obtained recirculation zone is significantly smaller than in the k-ε model (Figures 22 and 23). The location and the vortex dimension downstream the return vaned channel (Figure 24) differ in both the cases and in the k-ω model occupy more space.

5. Turbine blading redesign

The CFX-TASCFLOW code can be used in the turbine blading design as well. In the design process of the turbine stage with cylindrical blades, ideal rotor inflow conditions are assumed at the mean radius. It means that the rotor inflow conditions are not optimal at the hub and at the blade tip. Since the 1930's twisted rotor blades (free vortex rule $c_u r = const.$) have been used in the rotor blade design. The rotor inflow conditions have been improved thus. However, the free vortex rule provides significant differences in the flow parameter distributions in the gap between the stator and the rotor. That was the reason why designers have been looking for other methods of twisting. There are many simpler methods of blade twisting, but the CFX-TASCFLOW as a checking method is in that case necessary. 3D codes allow one not only to get proper rotor inflow conditions, but to achieve proper pressure distributions as well. The computations have been made using the CFX-TASCFLOW code. The following boundary conditions have been assumed: total pressure at the stage inlet, static pressure at the outlet, frequency and mean velocity at the inlet. The k-ω model has been used with the turbulence intensity about 5%.

Figure 25. Two different kinds of rotor blades: left – cylindrical, right – twisted

In Figure 26 the working medium flows exactly on the blade inlet edge for $x/L = 0.2$, and for $x/L = 0.8$ it flows on the suction side of the blade (it means the intersection point of the profile inlet arc and the camber line of the airfoil section is a stagnation point – the optimal conditions of the flow around the profile).

In that case a strong separation region appears at the pressure side in the region close to the blade tip.

The numerical investigations of the clocking effect in a two-stage air model turbine are now conducted at the Institute of Turbomachinery. The calculations are made for several different rotational speeds and for two different types of the turbine design: TM3.0 (old version) and TM3.11 (new-concept design with a lower number of rotor blades). The TM3.11 turbine has been optimised using the CFX-TASCFLOW code.

In Figure 27, the inflow view on rotor 1, stator 2, rotor 2 and circumferentially averaged angles α and β and velocities c and w for the TM3.11 turbine are presented.

In these figures, one can see not only how the wheel inflow changes, but also how circumferentially averaged distributions vary along the blade height. A correction
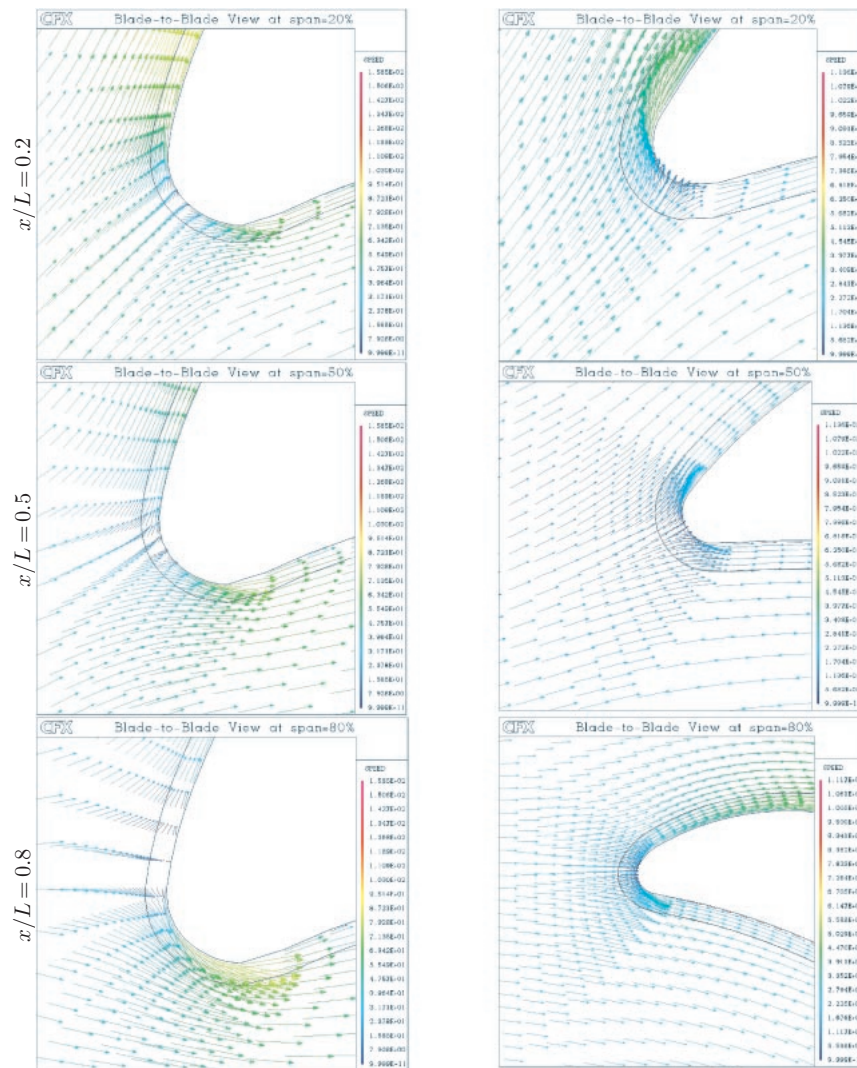
Figure 26. Velocity vector distribution for the rotor in the blade-to-blade cross-section
for 20, 50 and 80% of the blade height

of the channel shape is possible in the design process through a change in the profile
shape or its position. In the case under consideration, a profile position of the second
rotor has been changed.

A tool like CFX-TASCFLOW allows one to shape turbomachinery flow channels
in a simple and arbitrary way and to observe if these changes do not generate
disadvantageous phenomena.

The CFX-TASCFLOW code is used by biggest companies. In 1998 Siemens
AG and VEM Kernkraftwerk Emsland modernized the LP part of a huge steam
turbine. They used new TX profiles and reduced the number of LP stages from 10 to
8 (Figure 28). The results were even better than the designer's expectations (Figure 28
– upper right corner).

Strictly correct loss values are not so important in this case. In Figure 29 the streamline shape before and after modernization is presented. In a new version of the stage, the streamlines close to the hub are uniformly distributed. It means that there is no separation in the hub region. CFX-TASCFLOW allows for influencing flow phenomena. It is important to know that the causes of loss generation are removed, the exact value of losses is not very much significant in the design process.

6. Conclusions

The necessity of using CFD codes for better designing of different kinds of turbomachines was proved. The design process of the modernized radial compressor stage by using the CFX-TASCFLOW code was presented. The designer had a really difficult task. The new operating conditions of the compressor were completely different from the original ones, but the dimensions of the casing and the rotational speed could not be changed. The first analysis of the compressor designed by the 1D methods shows a separation region starting in the half of the meridional channel. Because of the mass flow requirements the channel was made insignificantly wider at the inlet and the channel curvature was changed. It significantly improves the flow in
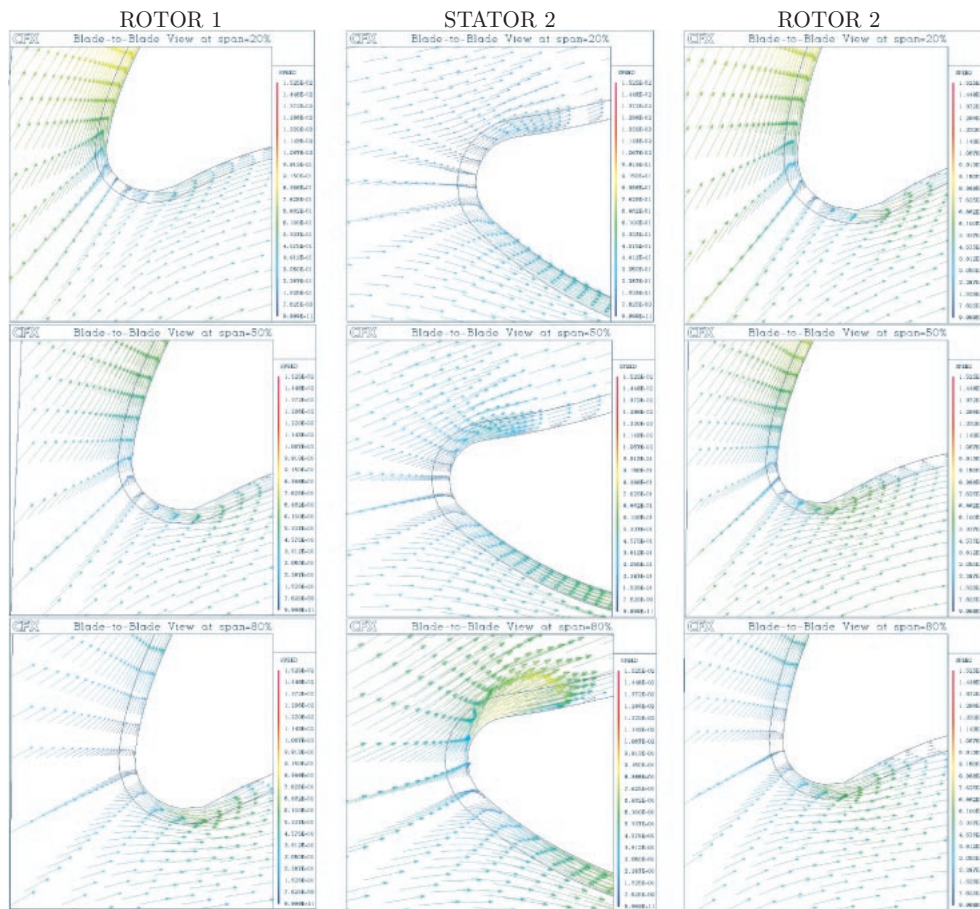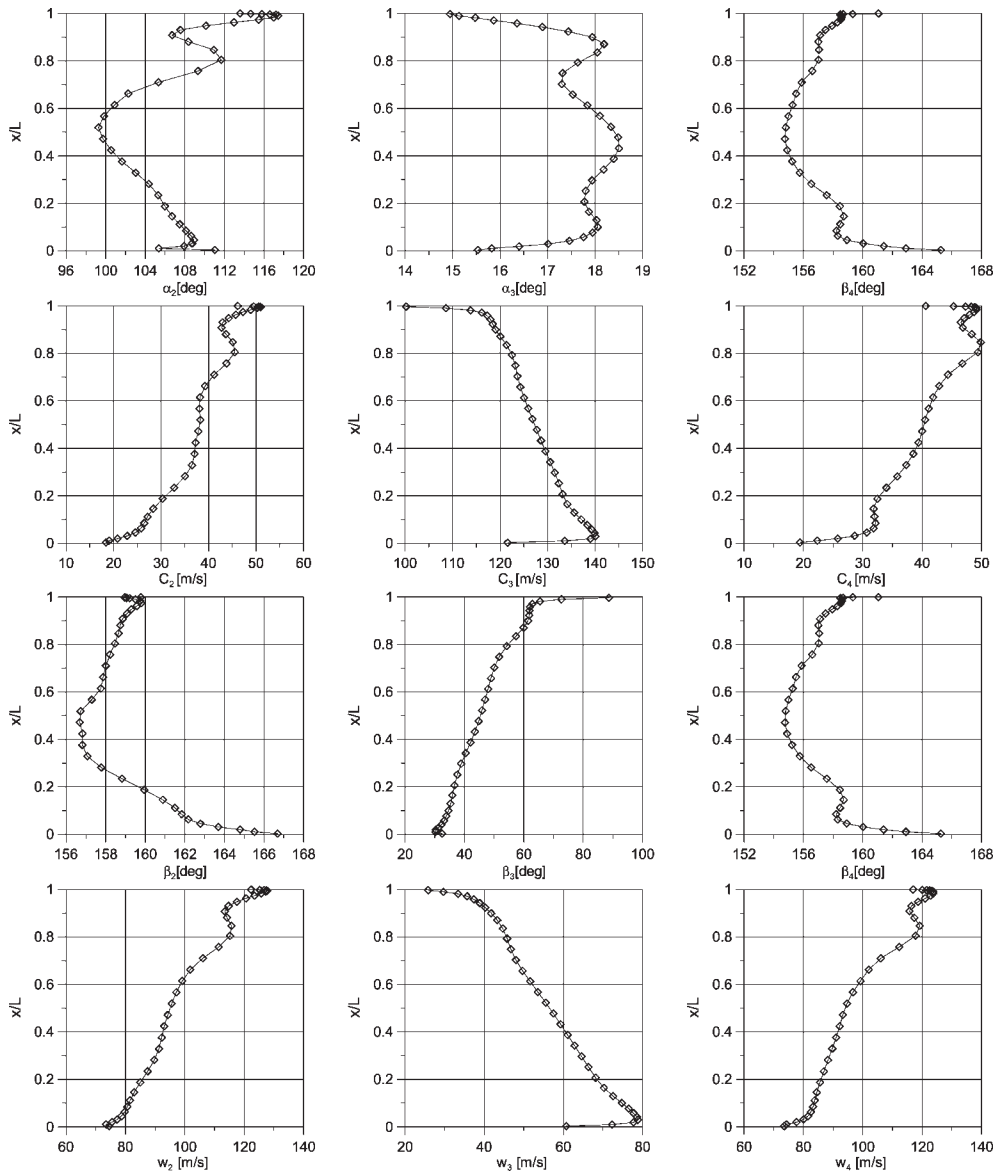

(Continued on the next page)

Figure 27. Velocity vector distribution at the rotor in the blade-to-blade cross-section for 20, 50 and 80% of the blade height and α, c, β, w radial distribution

the whole stage. The code was used for the steady calculations of the compressor to recognize phenomena responsible for surge. The inlet recirculation, separation in the vaneless diffuser and separation in the rotor channel were recognized. In the authors opinion the proposed way can be successfully used for the prediction of unstable operating conditions of a compressor without a necessity of unsteady calculations (especially important for a person using PC class computers in the design process). The understanding of flow phenomena is a key point for changes made in the channel and blades shape; *e.g.* the appearance of the inlet recirculation means a necessity of making the channel more narrow not only at the inlet, like in the previously mentioned
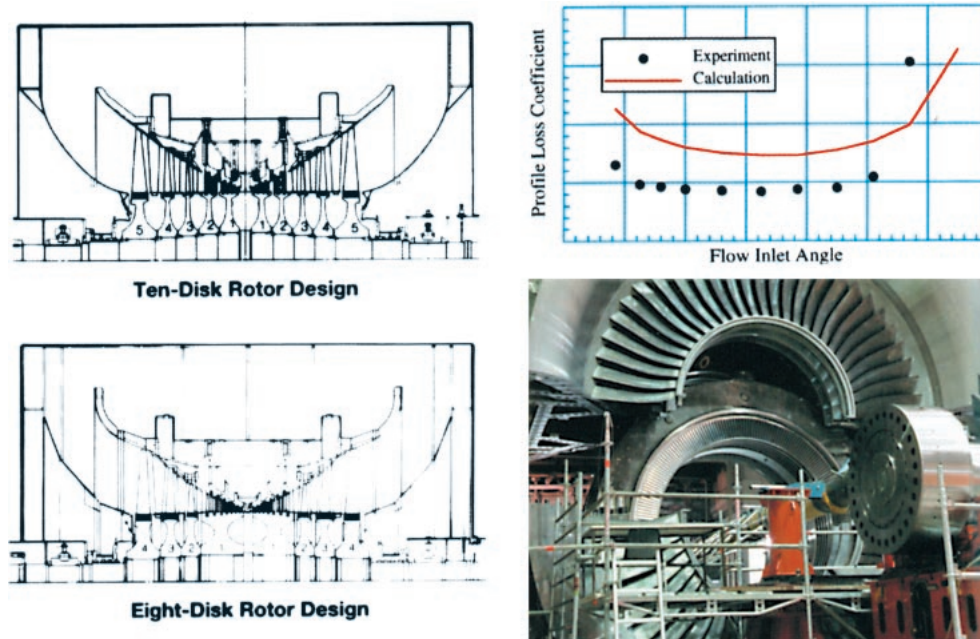
Ten-Disk Rotor Design

Eight-Disk Rotor Design

Figure 28. LP part of the steam turbine before and after modernization [10]
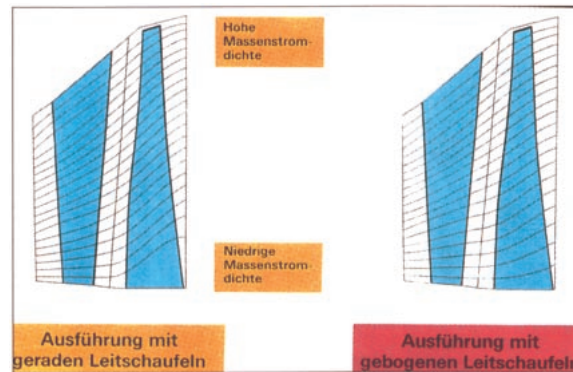

Figure 29. Streamline location before and after modernization [10]

case, but at the outlet as well. The CFD codes are really useful and sometimes it is not so important to get an excellent accuracy of the efficiency calculations, but the possibility of observing flow phenomena in a way unavailable in measurements techniques.

Acknowledgements

References

[1] 2000 CFX-TASCflow, *Computational Fluid Dynamic Software, Primer Documentation*, Version 2.10, 2000 by AEA Technology

[2] Chodkiewicz A 1995 *Investigations of Compressor Characteristics at Unstable Operation*, MSc. Thesis, Institute of Turbomachinery, Technical University of Lodz, Poland (in Polish)

[3] Kryłłowicz W and Turbine and Compressor Team of Technical University of Lodz 1995 *Complex Investigations of Compressors with Adjustable Diffusers and Stators Integrated with Gear Box*, Report No. 9 as S6 03 02204, Report No. 1307 of Institute of Turbomachinery, Technical University of Lodz, Poland (in Polish)

[4] Kryłłowicz W, Horodko L and Hanausek P 1996 *VDI Berichte* **1249** 413

[5] Kryłłowicz W and Hanausek P 1998 *Proc. 8th Int. Conf. Fluid Flow Machinery*, Rzeszow-Bystre, Poland, pp. 238–246 (in Polish)

[6] Breugelmans F A E and Sen M 1982 *Proc. 11th Annual Turbomachinery Symposium*, Texas University, USA, pp. 165–180

[7] Japikse W, Carter A and Swardsen M 1980 *Improvements in Surge Margin for Centrifugal Compressors, Centrifugal Compressors, Flow Phenomena and Performances*, AGARD CP 282, Paper 13

[8] Błaszczyk A, Staniszewski J, Najdecki S, Paperski A and Woźniak D 1994 *Flow Investigations of Multistage Centrifugal Pumps*, Report of Institute of Turbomachinery, Technical University of Lodz, Poland (in Polish)

[9] 1997 *TECPLOT User Guide*

[10] Oeynhausen H, Classen H P and Riehl J 2001 *Dampfturbinen-Service. Wirkungsgrad verbessernde Maßnahmen im Kernkraftwerk Emsland*, BWK **53** (5)